Received December 12, 2020, accepted December 24, 2020, date of publication January 5, 2021, date of current version January 13, 2021.

*Digital Object Identifier 10.1109/ACCESS.2021.3049170*

# A New Diagnostic Technique to Detect Early Migration of Joint Prostheses

**MUHAMMAD MOID KHALID KHAN[1], SUBODH C. DESHMUKH[1,2,3], KANTHAN THEIVENDRAN[1,2], LAURA J. LESLIE[1], AND SARAH JUNAID[1]**

[1]School of Engineering and Applied Science, Aston Institute of Materials Research, Aston University, Birmingham B4 7ET, U.K.
[2]Sandwell and West Birmingham Hospitals NHS Trust, Birmingham B71 4HJ, U.K.
[3]The Royal Orthopaedic Hospital NHS Foundation Trust, Birmingham B31 2AP, U.K.

Corresponding author: Sarah Junaid (s.junaid@aston.ac.uk)

This work was supported in part by the Aston University, and in part by the Trauma and Orthopaedic Department, Sandwell and West Birmingham Hospitals NHS Trust.

**ABSTRACT** Migration of an implanted prosthesis due to aseptic loosening is difficult to detect without regular imaging. In this paper, a low-cost, non-radiographic, robust diagnostic technique is presented, which can detect the migration of the humeral component of an elbow prosthesis. The system consists of a single magnet single sensor configuration and migration data are based on the variation in the magnetic field. The magnetic sensor was enclosed in titanium alloy and a magnet was embedded at a reference point in the humeral bone enclosed in ultra-high molecular weight polyethylene (UHMWPE). A layer of bone cement was then placed between the enclosed magnet and sensor. An algorithm linked with a Savitzky- Golay (SG) filter was developed that could decouple, convert, and filter the magnetic field signal to provide both the linear and angular displacement. The system was also designed to eliminate the cross talk and non-linearity effect of the magnet. The highest resolution the sensor achieved was 0.3 mm with a detectable linear migration range of 0.3 mm to 4 mm in the x/y axis and between 8-20 mm in the z-axis (along the humeral canal). The detectable rotational range was 0.5 to 3.0 degrees in the x/y axis. The repeatability of the calibrated sensor was analysed and showed a standard deviation of 0.05 mm over 150 cycles. The resolution was dependent upon the operating conditions and sensor positioning. There was no interference from the titanium alloy, bone cement nor the UHMWPE. This sensor system offers an alternative non-radiographic option for measuring migration of implanted prostheses.

**INDEX TERMS** Aseptic loosening, sensor calibration, Savitzky–Golay filter, low cost, and non-radiographic.

## I. INTRODUCTION

Aseptic loosening of the elbow prosthesis is considered to be the key contributor in the failure of total elbow arthroplasty (TEA) [1]–[5]. A study investigating TEA from the Finnish nationwide joint registry publication shows that 47 % of revision surgeries are carried out because of aseptic loosening [6]. In almost all types of elbow prostheses, aseptic loosening is the leading cause of revision surgeries, affecting the longevity of the prostheses [7]–[10]. In comparison, the 10-year survival rates of total knee (TKA) and hip arthroplasties (THA) are reported at 90 % and 95 % respectively [5], [11], [12] with the survival rate of TEA being 79.2 % [5].

Early detection of loosening is key to identifying early bone loss and the ''silent failure'' often seen in TEA as well as reducing the clinical burden and financial implications. However, detecting, diagnosing, and monitoring early aseptic loosening remains a challenge [1]–[12].

The associate editor coordinating the review of this manuscript and approving it for publication was Yasar Amin.

### A. CURRENT DIAGNOSTIC TECHNIQUES

X-ray imaging (plain radiographs) is currently used in clinical practice to detect loosening at regular time intervals (e.g. every 6 or 12 months). However, detection of early stages of loosening are ambiguous and can be subjective due to low specificity and accuracy [13], [14]. This limits the use of X-ray techniques in detecting early loosening, although it is considered the gold standard in confirming implant loosening. Different imaging modalities have also been carried out in detecting prosthesis loosening which include arthrography, bone scintigraphy, magnetic resonance imaging (MRI) and 18-fluorodeoxyglucose positron emission tomography (FDG-PET). The main difficulty in these techniques is that their detection performances are variable, they are time consuming, interpretation of the results is difficult and

observer-dependent, and they are costly which makes them an inappropriate tool for detecting early migration of the prosthesis [15]–[17].

One high precision radiographic method for detecting aseptic loosening is the Radio Stereometric Analysis (RSA) technique [18]. RSA can measure early signs of prosthesis displacement within the first postoperative year. However, this technique can only be adopted as a clinical research tool and can only be used in a small number of patients. There are also a limited number of studies on RSA of the elbow joint compared to hip and knee [19], [20]. One of the main reasons behind this is the symmetrical shape of the elbow prosthesis and the limited size of surrounding bone, which leads to over projection [18]. The mean precision of the studied elbow prosthesis migration was 0.29 mm translational and 0.66° rotation for the humeral component [20]. Another drawback of RSA is the requirement of x-ray exposure.

Vibrometery is another technique (contact based) that is currently being used in TKAs and THAs to detect loosening, which is based on measuring the propagated vibrations of the tibia component using 3D accelerometers, but this technique has only 20% higher sensitivity and specificity than radiographs and has never been used in elbow prostheses [14], [17], [21].

### B. SMART IMPLANTS

Considering the above-mentioned detection techniques, their limitations and the complication rate of TEA which is 20-40 % more than TKA and THA [20], a substitute method is required. The substitute method for detecting aseptic loosening is to embed sensors in existing prostheses (with minimal modification of implant design) making the prostheses ''smart'' or ''instrumented''. Embedding sensors in prostheses has been performed in other joints to measure force, kinematics, and temperature. The first instrumented prosthesis was designed for the hip by Bergmann *et al.* (1993), which included strain gauges to measure force [22]. Similar sensors were designed for the knee to measure the tibiofemoral compression force. Recently, a smart instrument design for the knee prosthesis has been developed for estimating the kinematics of knee prostheses during different movements. Also, another instrumented knee prosthesis is developed with self-powered force measuring capabilities [23], [24]. No instrumented prosthesis has been designed for the TEA that can monitor the prostheses performance to our knowledge to give feedback. A magnetic field measuring system, which has been used broadly for positioning sensing in automation industries and for contactless movement in harsh environment [25], is another technique that can potentially be used in a prosthesis for motion or loosening detection. Magnetic sensor can be divided into two types based upon their excitation (coils and magnets). The sensors are fabricated in way to output orthogonal signal with respect to magnetic field [25], [26]. Recent advancement in magnetic sensor design has worked on providing low power, small size, and high-resolution sensors to estimate the intensity and orientation

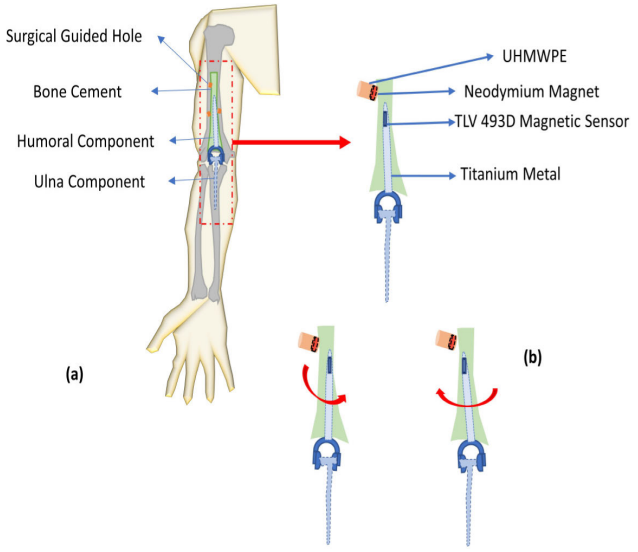


**FIGURE 1.** (a) Proposed diagnostic system overview (b) Sensor and Magnet placement in the system.

of a magnetic field [26]. Due to the transparency of the human body to magnetic fields, these sensors are suitable for embedding in a prosthesis. A limited number of studies have been carried out on embedding magnetic sensors in prostheses to detect kinematics and force [23], [27]. To the best of our knowledge, no one has used this technique to detect the migration of the prosthesis from its original position and therefore provide early diagnosis of aseptic loosening.

In this work, we present a low cost, non-contact, X-ray-free technique to detect migration of the humeral component of an elbow prosthesis. A simple calibration method is used to decouple the raw magnetic field data into migration parameters, namely static and dynamic, and a standard filtering procedure is used to eliminate the high frequencies content in the calibrated signal.

The rest of this paper is constructed as follows: Section II, the overall system description and methodology, Section III outlines the experimental results, Section IV outlines the discussion and Section V the conclusion.

## II. METHODS

### A. DIAGNOSTIC SYSTEM OVERVIEW

The proposed diagnostic technique used for detection of aseptic loosening of the elbow prosthesis is shown in figure 1.

The measuring system consists of a sensory component and magnetic component. The sensory component is a 3-axis magneto-resistive sensor, which is embedded in the humeral stem of the elbow prosthesis, made of cobalt-chromium (ASTM F75) or titanium alloy (Ti-6Al-4V). As these metal alloys have negligible effect on the magnetic field [27], the sensor will be able to detect the magnetic field without any attenuation. The magnetic component (axis-magnetised magnet) placed at a reference point through Surgical guide holes in the humeral bone. The magnet is enclosed in UHMWPE and acts as a source for detecting any translational or rotational loosening.

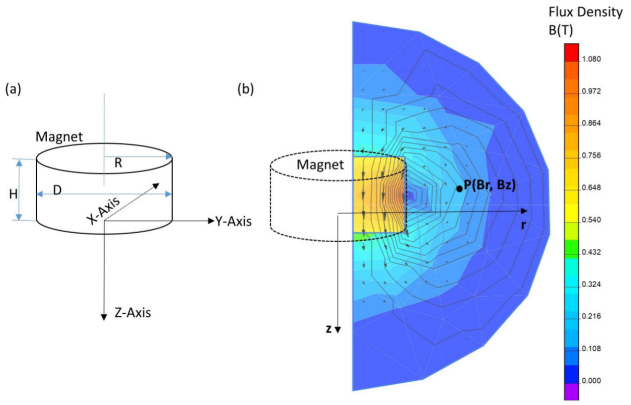


**FIGURE 2.** (a) Cylindrical magnet dimension. (b) Magnetic field (B) of cylindrical magnet in z-r plane.

Finally, the area between the sensor and magnet is filled with bone cement and body tissue or fluid. The sensor detects the magnetic field emitted from the magnet and the raw data is sent to a PC via a USB cable. A software program written in LabView (National Instruments, Austin, TX, USA) and MATLAB (The Mathworks Inc., Natick, MA, USA) calculates the position of the humeral stem relative to the magnet.

The fundamental idea behind this diagnostic technique is the calculation of the distance between the magnet and sensor, based on the magnetic field measurement detected by the sensor. Figure 1 highlights the position of the sensors that will be responsible for detecting any micro motion along the three axes. Also, the magnetic field decays with distance from the magnetic source, however this decay is unaffected by human tissue or biomaterials (titanium alloy, cobalt chromium alloy, UHMWPE and PMMA bone cement). Furthermore, the human body has shielding properties that has been shown to be identical to free space [28].

### B. MAGNETIC FIELD DISTRIBUTION

The remanence of the magnet depends upon on the magnet's size, material, forming process and temperature which have been kept constant in this study. In this section, the magnetic field of an axis-magnetised cylindrical magnet was investigated to obtain the magnetic position sensor behavior. According to Schott *et al.* (2002), whenever a magnet is displaced from its original position, the relevant direction and distance between the sensor and magnet changes, which is equivalent to the displacement of the sensor in the magnet field of a magnet with a fixed position [29].

The selection of magnet size was limited by its insertion in the humeral bone. The magnet selected for this study was a rare earth neodymium (NdFeB-42) which provides the highest available remanence to size ratio [28]. Figure 2a shows the dimensions of the cylindrical magnet with diameter of 7 mm and a height of 3 mm.

To investigate the magnetic field of the magnet an axisymmetric finite element model was used to simulate the magnetic field (Quick Field 6.3.1.2049, Tera Analysis Ltd., and Svendborg, Denmark). The simulation of magnet was investigated in an air medium have a relative permeability of 1. The permeability of the magnet was selected based on the coercive force 9300 A/m and the remanence flux density of 11300 of the magnets. The mesh size of 250 was selected. Figure 2b shows the magnetic field vector distribution in the z-r plane. As the simulated magnetic field is axisymmetrical the 3D model can be described in 2D map. The magnetic field at any point P in the 2D map can be calculated by using equations (1)-(5) as described in detail by Schott e al. (2002) [29]. The validity and application of these equations to determine distance as a function of magnetic field is described in the paper, where the authors report experimental errors as low as 10-40 $\mu$m (0.5 – 2 % error) at 0 to 2 mm testing range [29].

$$\frac{B_x}{B_y} = \frac{x}{y} \tag{1}$$

$$B_r = \sqrt{B_x^2 + B_y^2} \tag{2}$$

$$r = \sqrt{x^2 + y^2} \tag{3}$$

where $B_x$ and $B_y$ are the magnetic fields measured in x-y axis, x and y are the coordinate positions, $B_r$ is the magnetic field in the x-y plane and r is the radius in the x-y plane. Thus, the coordinate of the magnetic field at point P can be calculated in the 2D model by using the following equations, which have been derived previously [29]:

$$x = r.\frac{B_x}{B_y} \tag{4}$$

$$y = r.\frac{B_y}{B_x} \tag{5}$$

So, to obtain the three-axis displacement of the sensor from the three-axis magnetic field the relationship between ($B_z$, $B_r$) and (z, r) is enough where $B_z$ is the magnetic field in the z-axis.

### C. MAGNETIC SENSOR SELECTION

The different types of magnetic sensor techniques include: Hall Effect, anisotropic magnetoresistance (AMR), giant magnetoresistance sensor (GMR), Flux gate effect, induction coil effect, MEMS Lorentz force and other magnetic phenomena, which has the capability to measure the magnetic field with resolution from pico Tesla (pT) to milli Tesla (mT) with a bandwidth from DC to MHz. The performance of these technologies used in different magnetic sensors can be found in Lenz & Edelstein 2006 [30]. Among all these techniques and technologies, the Hall Effect sensor is most commonly used [31] in industrial applications (current sensing, proximity sensing, and position sensing) because of their compact size, low cost and ability to easily integrate with any data acquisition system. When a Hall Effect sensor is subjected to any magnetic field, a Lorentz force deflects the charge carriers resulting in a potential difference.

Now commercially available Hall Effect sensors can measure the magnetic field in 3- axes by utilising very low power. The sensor also includes a temperature sensor for thermal

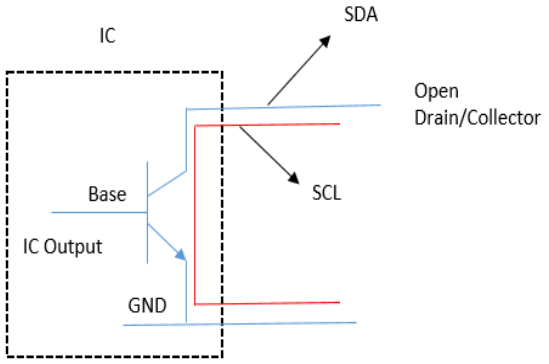


**FIGURE 3.** Sensor open drain configuration block diagram.

drift compensation and digital output via I2C or SPI bus to integrate with data acquisition. All these are embedded on a single chip typically 3 mm x 3 mm x 1 mm size.

### D. CONFIGURING THE MAGNETIC SENSOR SELECTION

In this study the Infineon TLV493D magnetic sensor was used to detect magnetic field intensity in 3 orthogonal directions and from this, the prosthesis position can be determined. The printed circuit board (PCB) was designed for the sensor and then the PCB was enclosed in 2 mm thick titanium alloy (Ti-6AL-4V). Before calibrating the sensor according to our working envelope, the sensor needed to be configured with the data acquisition device, since this sensor is a digital sensor and it utilises an I2C communication protocol. Here we have used NI MyRio as a data acquisition device to retrieve data from the magnetic sensor via its SDA (Serial Data pin) and SCL (Serial Clock pin). As the magnetic sensor has the output via I2C protocol, two pull up resistors were required on the I2C line (SDA and SCL) as shown in figure 3. These resistors are necessary because the device has an open-collector configuration.

In open collector configuration, the system can only connect to the clock line (SCL) or signal data line (SDA) to the ground but it cannot drive the lines to high. For the line to be able to go to the high voltage the pull-up resistor must be inserted because we need a stable voltage state to define the two-binary state of bits i.e. 0 V as 0 bit and 3.3V as 1 bit.

The value of the pull-up resistor is important for the design configuration because an incorrect value of the resistor can lead to signal loss. By using the following equations the values of the pull-up resistor can be calculated [32].

$$R_{min} = \frac{V_{cc} - V_{OL(Max)}}{I_{OL}} \tag{6}$$

where $R_{min}$ is the minimum pull up resistor value, $V_{cc}$ is the supply voltage, $V_{OL(Max)}$ and $I_{OL}$ are low-level output voltage and current respectively.

$$R_{max} = \frac{t_r}{0.8473 * C_b} \tag{7}$$

where $R_{max}$ is the maximum value of the pull-up resistor, $t_r$ is the rise time and $C_b$ is the bus capacitance. Therefore, the pull-up resistor value can be selected between $R_{min}$ and $R_{max}$.

The next step was retrieving data from sensor specified registers as the magnetic sensor consists of 4 sensing elements (3 hall plates and 1 temperature sensor). Their data is stored in a specific register as described in the sensor bit map. Each register can store up to 8 bits of data but for the correct magnetic field value, the sensor must measure 12 bits of data. To achieve this, an appropriate code was written in LabView, which can read the data from the specific register and arrange it into 12 bits of data.

### E. BONE CEMENT PREPARATION

PALACOS (Heraeus Noblelight Ltd, UK) low viscosity Polymethylmethacrylate (PMMA) bone cement[33] with and without antibiotic (Gentamicin) was used for this study. In TEA the low viscosity cement is commonly used with or without antibiotics depending upon the surgeon's preference [34]. The bone cement comes in two components made up of a powder (copolymer) and liquid (monomer). The cement was prepared as per the manufacturer's instructions. The two components were mixed together at a ratio of 2:1 in a bowl in a fume cupboard (Airone FC 750 model, Safelab systems Ltd. Somerset, UK) for 2-3 minutes to form PMMA cement. While in a semi-solid form, the cement was poured into a pre-made mould to make PMMA sections with thicknesses of 2.5 mm, 5 mm, and 7.5 mm. The PMMA cement was left in the mould for 5 minutes to completely polymerise and harden before removing from the mould.

### F. SENSOR CALIBRATION

A technique is defined for the calibration of the magnetic sensor which will be used to find migration of the implant relative to its original position. As the magnetic sensor has the capability of measuring magnetic field along three orthogonal axes simultaneously, the sensor can be used to measure field direction in two different planes. By using this concept, we can calibrate the sensor and identify its starting position. For the axis magnetised cylindrical magnet the magnetic field along its axis can be derived from Camacho [35].

$$B(z) = \frac{\mu_o M}{2}\left(\frac{z + H_m}{\sqrt{(z + H_m)^2 + \left(\frac{D_m}{2}\right)^2}} - \frac{z}{\sqrt{z^2 + \left(\frac{D_m}{2}\right)^2}}\right) \tag{8}$$

where $M$ is the magnetisation of the magnetic axially, $\mu_o$ is the relative magnetic permeability, $H_m$ is the height of the magnet, $z$ is the distance from the pole of the magnet and $D_m$ is the diameter to the magnet.

According to Chao Hu [36] the theoretical localisation of a magnet can be found by using the equation:

$$\begin{aligned} Bz &= Bx + By + Bz \\ &= \frac{\mu_o M}{2}\left(\frac{z + H_m}{\sqrt{(z + H_m)^2 + \left(\frac{D_m}{2}\right)^2}} - \frac{z}{\sqrt{z^2 + \left(\frac{D_m}{2}\right)^2}}\right) \end{aligned} \tag{9}$$

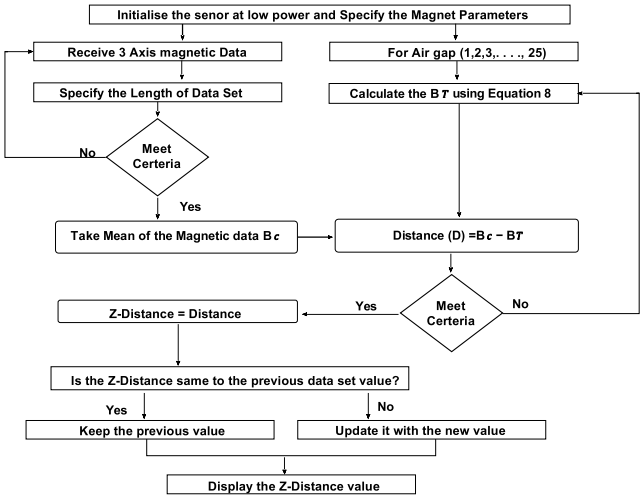


**FIGURE 4.** Flow chart of the proposed algorithm.

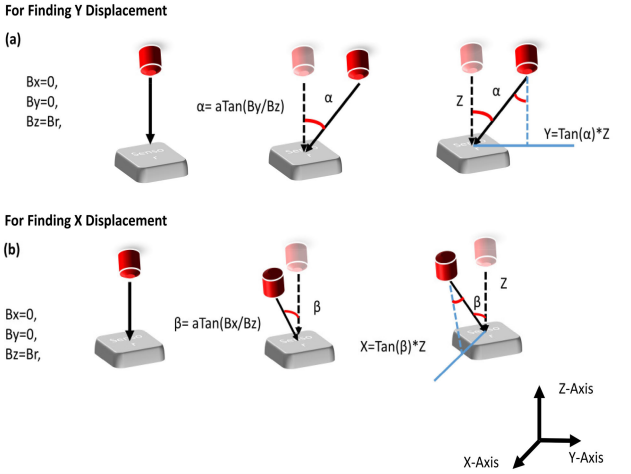


**FIGURE 5.** (a) Linear/ Angular movement detection mechanism in Y-Axis. (b) ) Linear/ Angular movement detection mechanism in X-Axis.

where $(Bx, By, Bz)$ are the 3 components of the magnetic flux intensity of the magnetic sensor. In our study to find the distance from the measured magnetic field values, an algorithm was used as shown in Figure 4.

The magnetic field values from the sensor data are compared to the theoretical distance values as shown in the algorithm (figure 4). The algorithm looks for a match to identify the z distance between the magnet and the sensor. If at the value of z, the difference between the magnetic field and theoretical value is zero or close to zero that value of z will be considered as the distance between sensor and magnet. Once the z distance is determined, the linear/angular displacements in the x and y axes are determined (figure 5).

According to figure 5a, when the magnet is displaced in the Y direction it makes an angle $\alpha$ with respect to its previous position and wherever this change occurs only the magnetic field in the y-z axis changes. Similarly, in figure 5b, when the magnet is displaced radially (x-direction) it makes an angle $\beta$ by altering the magnetic field in the x-z axis. To find $\alpha$ and $\beta$ the following equations were used.

$$\alpha = \tan^{-1}\left(\frac{B_y}{B_z}\right) \tag{10}$$

$$\beta = \tan^{-1}\left(\frac{B_x}{B_z}\right) \tag{11}$$

To find the relative displacement of the sensor from its original position, $\alpha$ and $\beta$ angles will be multiplied with the Z distance (the distance between the sensor and magnet). That will yield the displacement of the sensor in the Y and X directions.

$$Y\ Distance = \tan\alpha * Z\ Distance \tag{12}$$

$$X\ Distance = \tan\beta * Z\ Distance \tag{13}$$

### G. SIGNAL FILTERING TECHNIQUE

The data received from the sensor needs to be smoothed as it contains high-frequency content that cannot be removed by a plain FIR average filter. To achieve the high degree of noise removal from the desired signal, the length $(N)$ of the signal has to be larger so that the signal bandwidth becomes greater than the filter passband frequency [37].

$$\omega_c = \frac{\pi}{N} \tag{14}$$

In the current study, the Savitzky- Golay (SG) filter, also known as the least-square or polynomial smoothing filter, is used as a low pass filter to smooth the desired signal. [37]. The output signal, y(n), from the sensor can be represented as:

$$y\,(n) = x\,(n) + w(n) \tag{15}$$

where $x\,(n)$ represents the magnetic field signal with high-frequency content while $w\,(n)$ is the associated noise with magneto resistive sensor i.e. Johnson (thermal noise), shot noise, 1/f (flicker) noise.

The SG filter can be defined by two parameters that are denoted as $K$ for the polynomial degree and $M$ for the sequence. The following assumptions are made in the SG filter:

I. All data points of the signal should be natural numbers.
II. The length of the signal should be $N = 2M + 1$ and is odd for the sequence of $M$.
III. Data points should be positioned symmetrically about the origin $x_o$.

Considering the above assumptions, the polynomial constructed to fit the set of data can be described as:

$$p\,(m) = \sum_{K=0}^{n} a_K m^K \tag{16}$$

where $m$ is the $m^{\text{th}}$ point of the filter window, $p\,(m)$ is the constructed polynomial and $a_K$ is the coefficient of the polynomial. The least square fitting residual is used to minimise the error in the constructed polynomial which is described as follow.

$$\varepsilon_n = \sum_{m=-M}^{M} (p\,(m) - x\,(m))^2 = \sum_{m=-M}^{M} \left(\sum_{K=0}^{n} a_K m^K - x\,(m)\right)^2 \tag{17}$$

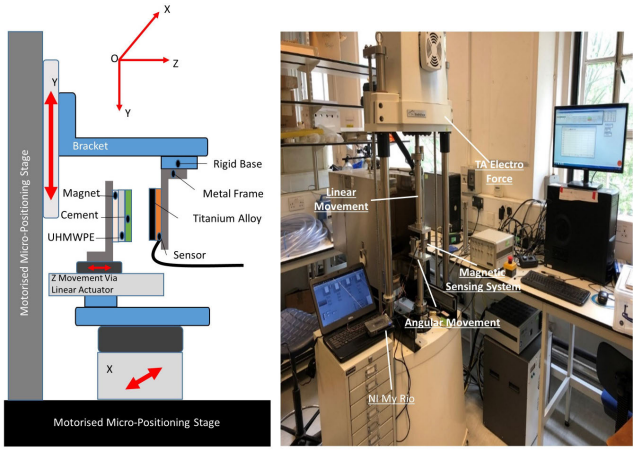


**FIGURE 6.** The schematics for test performance.

The SG filter shows that the process of filtering is equivalent to convolution of the sample around a window with a fixed impulse response. The resulting length $N$, order $K$, SG filter for smoothing a noisy sequence $x\,(n)$ will be, in its steady-state form equated as:

$$y\,(n) = \sum_{m=-M}^{M} b_0\,(-m)\,x(n-m) \tag{18}$$

where $b_0$ is the middle SG filter, as all data points should be symmetrical around the origin, $m$ is the $m^{\text{th}}$ point of the filter window and $n$ is the number of data point.

### H. PERFORMANCE TESTING

To evaluate the performance of the sensor and to obtain the correlation between the magnetic field and displacement, a mechanical testing system (Electro Force 3300, TA Instruments, Boston, USA) was used to provide input migration of the implant via its two motorised stages i.e. linear and rotational, with a resolution of 0.5 $\mu$m linearly, 0.01 degrees angularly and 0.01 Hz frequency. To provide a repeatable simulation of implant migration, we designed and fabricated an adjustable fixture/bracket for holding the sensor and magnet embedded in a UHMWPE. The fixture was attached to the Electro-force machine (see figure 6). The sensor bracket could be moved linearly in the y-axis and rotationally in the x-z plane. In order to move the magnet bracket linearly in the z-axis, an external linear actuator (P-16, Actuonix, Canada) was attached with a resolution of 1 mm and this was used to adjust the distance between the sensor and the magnet. The Electro-Force machine was programmed to move in the y-axis quasistatically (3-minute intervals) at amplitudes of 0.15 to 4 mm using square waveforms and dynamically using a sine waveform at 0.1 Hz. Rotational movement in the x-z plane was programmed quasistatically. The z-direction was controlled via the linear actuator, which was programmed using an external DAQ card (NI MyRio). The DAQ card was also used to communicate and acquire data with the sampling rate of 10 Hz from the magnetic sensor and to record data into a measurement file.

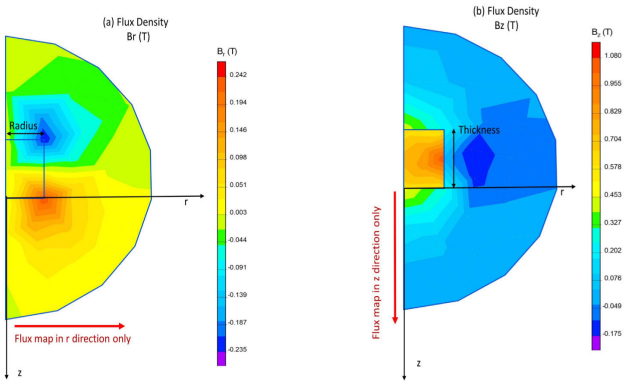


**FIGURE 7.** (a) Plane contour plot of a magnetic field in r-plane. (b) Contour plot in z-plane.

A paired t-test was carried out for each displacement position tested (0, 0.3, 0.5, 1. 1.5, 2. 2.5 mm) before and after applying the SG filter to test any significant changes to the raw versus filtered data sets from the filtering process. Also, the Levene's test was performed to check the homogeneity of variance. A non-parametric test was carried out using Linn's Concordance Correlation Coefficient.

## III. EXPERIMENTAL RESULTS

### A. MAGNETIC FIELD DISTRIBUTION

Figure 7 shows the contour plot of the magnetic field density of the magnet ($B_r$ and$B_z$) in the z-r plane. Figure 7a indicates that the value of $B_z$ increases when r is increased. It reaches its maximum value when r=Radius of the magnet, then $B_r$ decreases as r is increased and eventually moves towards zero. Also Figure 7b indicates that the value of $B_z$ decreases when z is increased and at distance z $>$ 20mm the value of $B_z$ is zero. To avoid multiple results when determining r and z from the magnetic field, it was determined that the movement of the magnet in the r plane should not exceed the specified regions as showed in the plots and all the movement should be restricted between these regions.

The Magnetic Flux density $B_z$ and $B_r$ of the cylindrical magnet in the z-r plan in figure 8 both show non-linear behaviour with increasing observation distance. Both $B_z$ and $B_r$ also show variability with change the z plane, which is the crosstalk effect.

### B. SENSOR CALIBRATION

Following the flow chart as describe in figure 4. The sensor was first calibrated in the z-axis only in order to estimate the distance between the sensor and magnet. The magnet was placed perpendicularly to the z-axis of the sensor (note that the North Pole was facing towards the sensor, if the poles change the magnetic field sign changes from positive to negative) and was moved linearly within the range of 8-20 mm at a step size of 1 mm. The resultant data set was processed with the algorithm as shown in figure 4 to determine the coefficients as shown in equation 12 and 13. Figure 9 shows the comparison of the estimated distance with actual distance. The estimated distance value is the average of 3 times

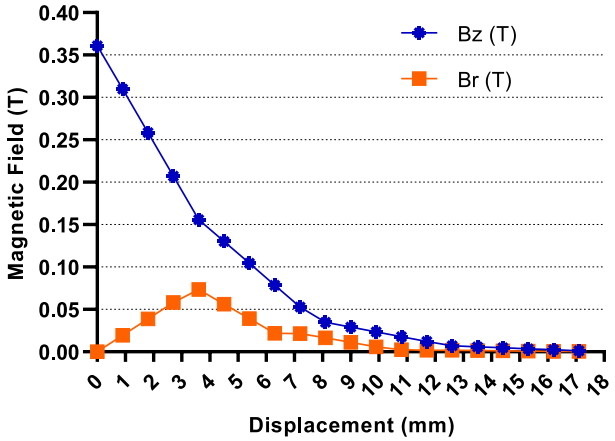


**FIGURE 8.** The magnetic field of the magnet in the z-r plane.

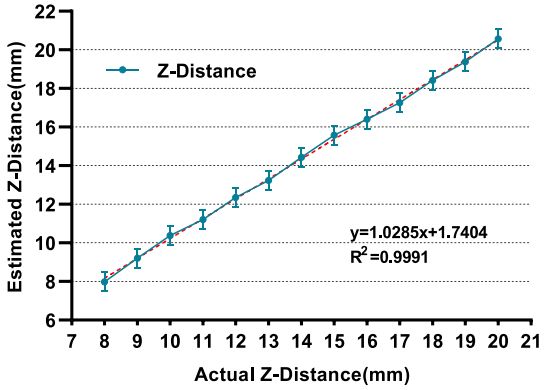


**FIGURE 9.** Validation of an algorithm to estimate the distance between sensor and magnet.

measurement and the error bars represent ± one standard deviation. The output of the estimated distance showed how well the algorithm fitted the actual value with an $R^2$ value of 0.9991. The standard deviation was less than 0.5 mm.

A similar set of experiments was conducted to analyse how the system will perform to detect the displacement of the sensor/magnet if they were moved in the other axes. The sensor was first moved linearly in the y-axis ranging from 0.1 mm to 4.0 mm with a step size of 0.5 mm (at z = 15 mm). Also, it was moved angularly around the y-axis ranging from 0 to 4.0 degrees. Figure 10 shows that the system was able to detect the displacement of the magnet in the y-axis with no change in the x or z -axis with a resolution of 0.3 mm. Displacement detection at different actual movements are provided in Table 1 for both filtered and unfiltered signals. The filtered version has a standard deviation of 0.079 mm as compared to the unfiltered standard deviation of 0.390 mm at 0.3 mm of displacement. A similar result was seen during the x-axis linear movement where the value does not change.

Table 1 shows both the raw and filtered signals have similar mean values with the filtered data showing lower variance (standard deviation). A paired t-test showed no significant differences between the raw and filtered data sets. Also, the Levene test shows that there is no homogeneity of variance between the raw and filtered data having $p < 0.05$.

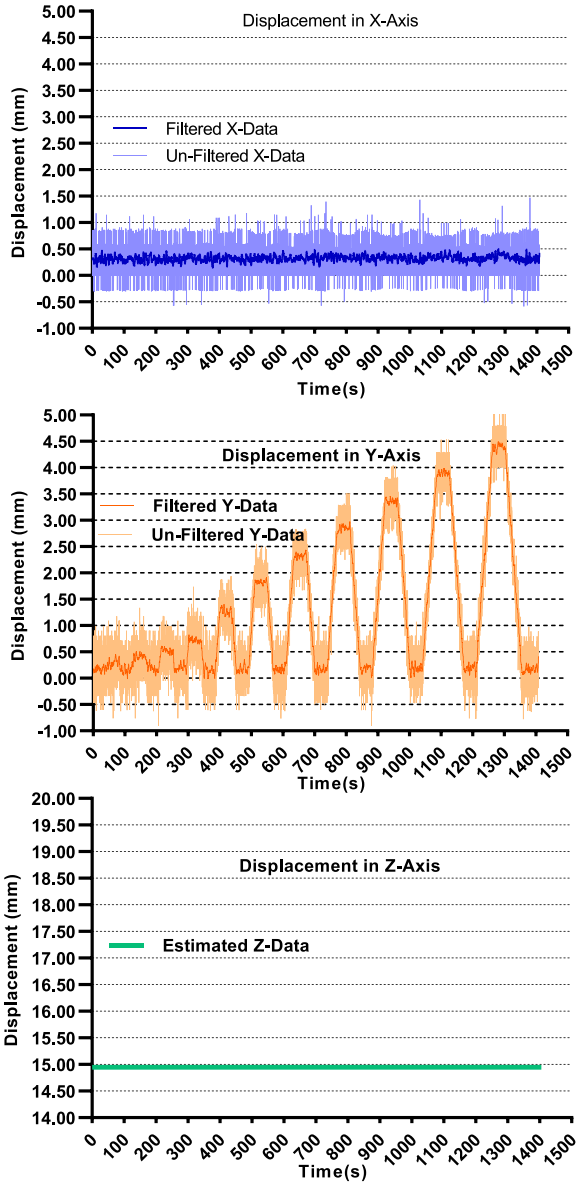


**FIGURE 10.** Quasistatic linear movement of magnet in Y-axis. Keeping X-axis position constant.

**TABLE 1.** Mean ± standard deviation of quasi-static linear movement of the magnet.

| Actual movement (mm) | Estimated Movement without filter (mm) | Estimated Movement with filter (mm) |
|---|---|---|
| 0.30 | 0.321±0.390 | 0.328±0.079 |
| 0.50 | 0.527±0.393 | 0.530±0.075 |
| 1.00 | 1.078±0.386 | 1.082±0.089 |
| 1.50 | 1.627±0.384 | 1.632±0.074 |
| 2.00 | 2.126±0.372 | 2.133±0.079 |
| 2.50 | 2.660±0.371 | 2.665±0.080 |
| 3.00 | 3.169±0.380 | 3.173±0.079 |
| 3.50 | 3.701±0.371 | 3.705±0.078 |
| 4.00 | 4.191±0.369 | 4.195±0.085 |

As, the assumption of homogeneity was not met. The non – parametric analysis Linn's Concordance Correlation Coefficient was performed. The analysis showed that the

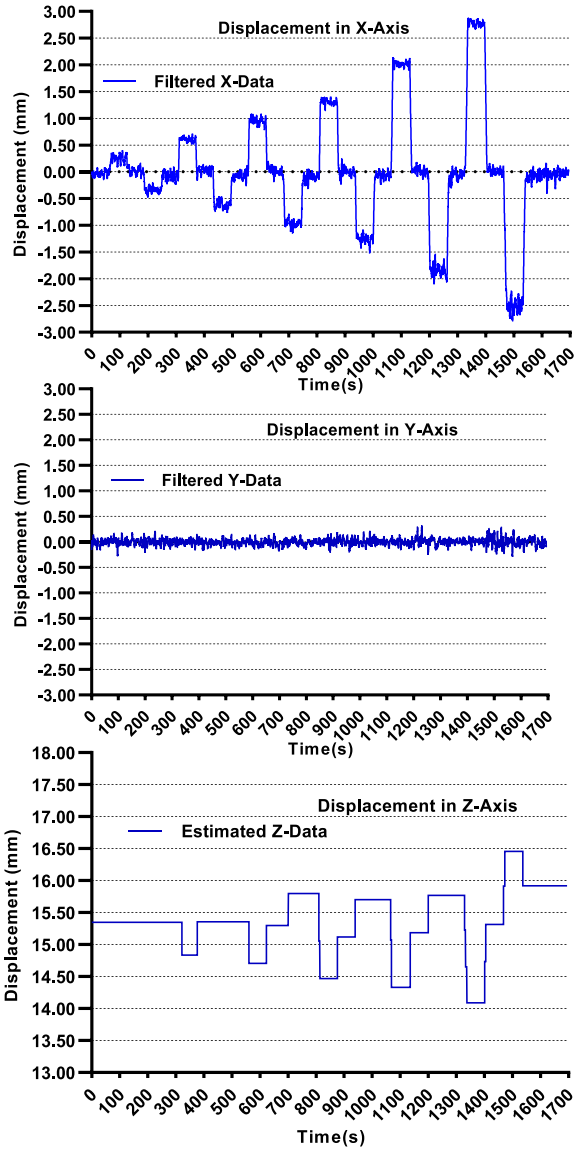


**FIGURE 11.** Quasi-static angular movement of the magnet in the X-axis. Keeping the Y-axis position constant.

filtered signal has strong concordance with the actual displacement (0.9913) while the unfiltered has a moderate (0.948).

Figure 11 shows the angular movement of the magnet around the sensor. The system was able to detect angular displacement up to 3 degrees (approximately 2 mm). Also, from figure 11 it can be observed that up to 1-degree rotation (1.2 mm angular displacement) there is no change in the Z-distance but beyond 1 degree the Z displacement starts to change depending upon the movement of the system

Also, it was observed that beyond 3 degrees the sensor was able to detect the magnetic field, but it introduced error in the tracking algorithm. This error was due to the tilting effect of the sensor.

Figure 12 (a, b) shows the comparison of the magnetic field ($By$) with the calibrated sensor output during the y-axis displacement at different z values. It was observed that during the y-axis displacement at different z values the magnetic

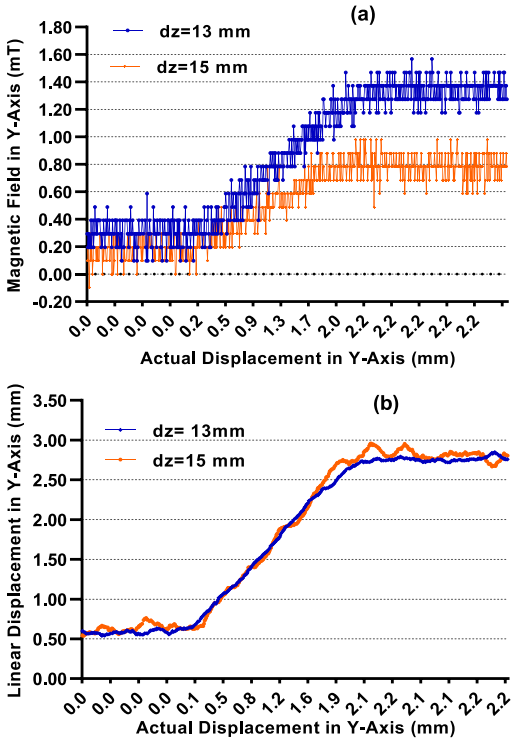


**FIGURE 12.** (a) $B_y$ during the y-axis displacement with different z values. (b) Calibrated Y Displacement output during different z values.

field ($By$) changes showing strong cross talk effect while the output from the calibrated sensor showed closed resemblance with the actual y-axis displacement across different z values, meaning that the cross-talk effect was eliminated.

Also, figure 13(a, b) shows that during z-axis displacement at different y displaced values, similar effects were observed with strong cross talk in magnetic field ($Bz$) and eliminated cross talk in calibrated sensor output in the z-axis.

### C. PERFORMANCE TESTING: DIFFERENT MOVEMENTS AND MATERIALS

The latter calibration steps were performed without introducing any material between the sensor and magnet. To further investigate the performance of the sensor, the system was tested by introducing different sets of the biomaterials that are presently used in the elbow prosthesis, namely, PMMA cement, UHMWPE and Titanium alloy (Ti-6Al-4V).

Also, to check the system performance under different migration parameters (dynamic and static) the system was moved dynamically at 0.1 Hz with the amplitude of 0.3 mm and then quasi statically with the same amplitude. Figure 14 shows that the sensor was able to detect both dynamic and static movement. Also, it shows that the biomaterials had a negligible effect on the measuring system.

Table 2 shows the displacement detected by the sensors at different movement under different biomaterials.

It was observed that under the static movement the calculated displacement is much more accurate having the error of 3.33% while in dynamic movement the error is of 10%.

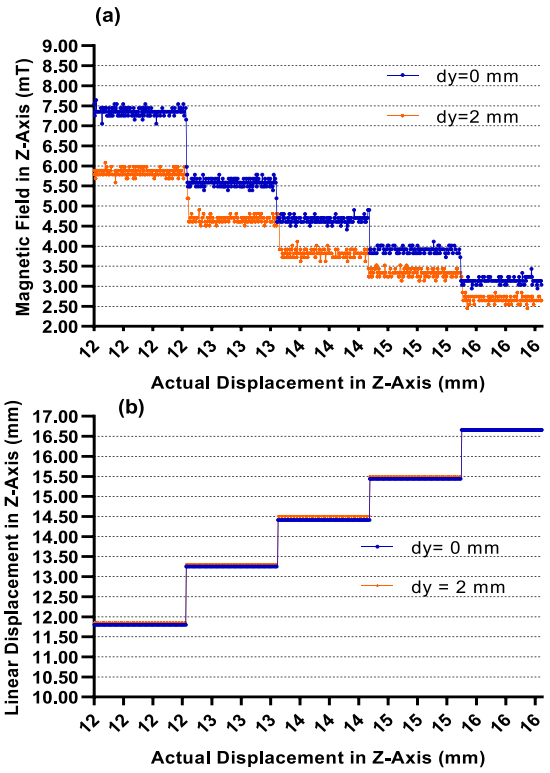


**FIGURE 13.** (a) $B_Z$ during the z-axis displacement with different Y displaced values (b) Calibrated z values during different Y displaced values.

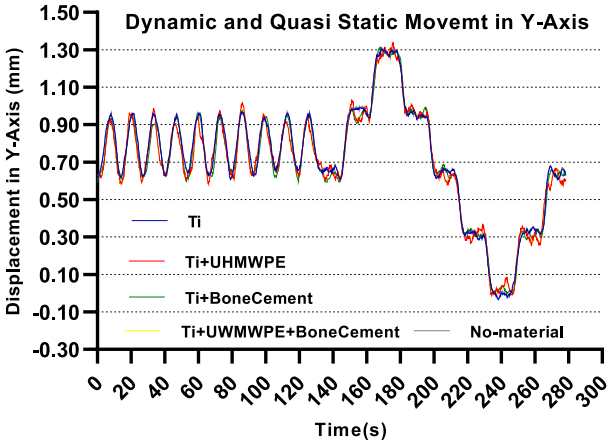


**FIGURE 14.** Performance of the system with different materials.

### D. PERFORMANCE TESTING: SENSITIVITY

According to the literature, there is no specific information on the minimum distance between the humeral component and surgical guide hole in TEAs. However, in the shoulder arthroplasty the minimum distance between the Guide hole and humeral component is 10 mm [38]. To check the sensitivity of our system we placed the reference point starting from 10 mm and showed the system performance under static and dynamic linear movement in the y-axis ranging from 0.15 mm to 1 mm. Figure 15 shows that as the distance between the sensor and magnet is increased, the resolution of the system decreases and more noise content is introduced to the signal.

**TABLE 2.** Mean ± standard deviation of static and dynamic movement at different material.

| Materials | Static Movement (0.3 mm) | Dynamic Movement (0.3 mm) |
|---|---|---|
| No Material | 0.3091±0.023 | 0.3133±0.1012 |
| Titanium | 0.3191±0.023 | 0.3231±0.1040 |
| Titanium and Bone cement | 0.3085±0.033 | 0.3305±0.1212 |
| Titanium and UHMWPE | 0.3043±0.028 | 0.3323±0.11175 |
| Titanium, Bone cement, and UHMWPE | 0.3085±0.033 | 0.3317±0.1221 |

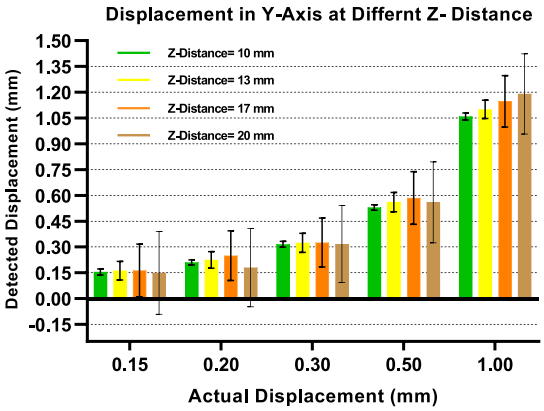


**FIGURE 15.** The sensitivity of the detecting displacement ranging from 0.15 to 1.00 mm at different Z-Distance.

Fig. 16 shows that at z = 13 mm, the system was able to detect accurately the static and dynamic movements. Beyond this distance, a 0.5 mm static movement was detected but with higher noise content. The results show that the ideal distance between the sensor and magnet for static and dynamic displacement should be below 17 mm.

### E. LINEAR AND ANGULAR MOVEMENT

Figure 17 shows that the system was able to detect linear and angular displacement simultaneously. As described previously, there was a change in the z-distance value when angular displacement exceeded 1.2 mm (1 degree). Also, if the sensor is not properly aligned to the magnet there is a small increment in the y-axis. Figure 17 also shows that the system was able to differentiate between linear and angular movement along with detecting changes in all axes.

## IV. DISCUSSION

Our system is based on the change in magnetic field of a magnet embedded in UHMWPE. The difference in the magnetic field measured by the sensor was used to detect loosening as low as 0.3 mm showing the ability to differentiate displacements in increments of 0.5 mm ($p < 0.05$).

Compared to the currently available technique, in which RSA is considered to be a gold standard for detecting aseptic loosening having a precision of 0.29 mm translation and 0.66° rotation [20]. However, it has downside of high cost, x-ray exposure and limited accessibility. The detection system presented here has several advantages over RSA and

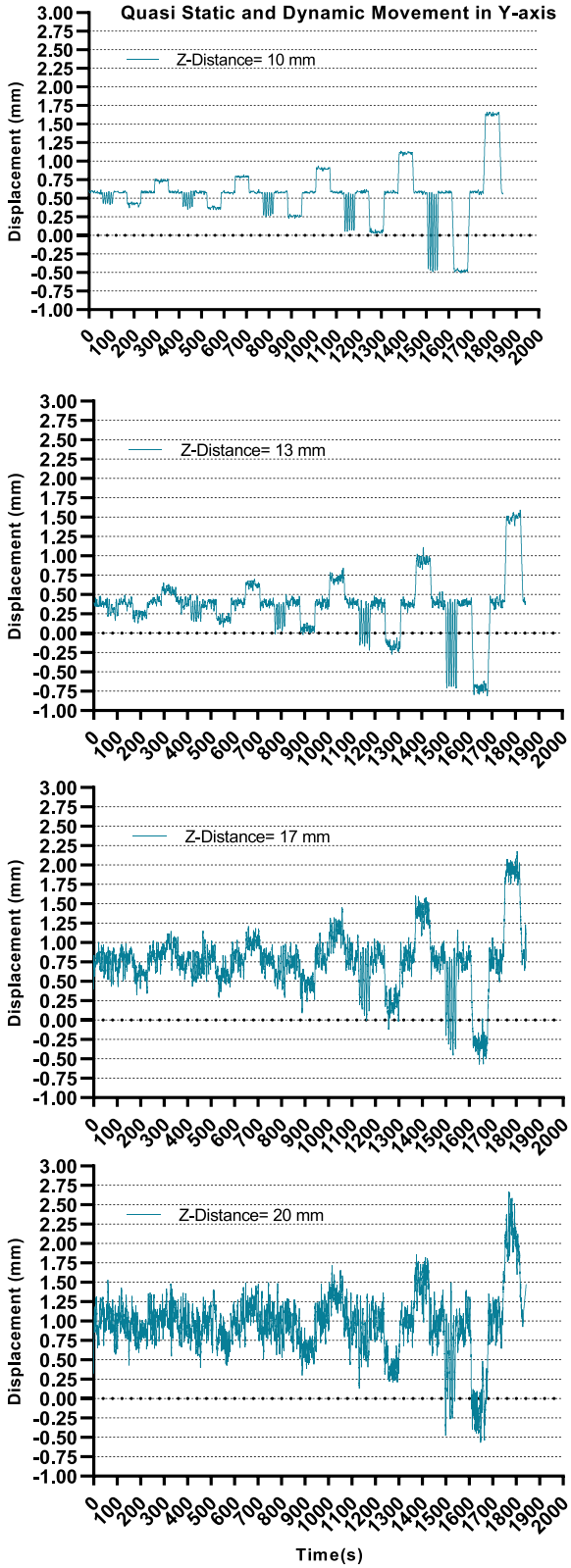


**FIGURE 16.** The sensitivity of the detecting system Quasi-Static and Dynamic at different Z-Distance.

other techniques (contact based), which include low cost, higher accuracy, non-contact, durability, measurement sensitivity and negligible effects from different materials (liquid and non-magnetic biomaterials). There are no systems to

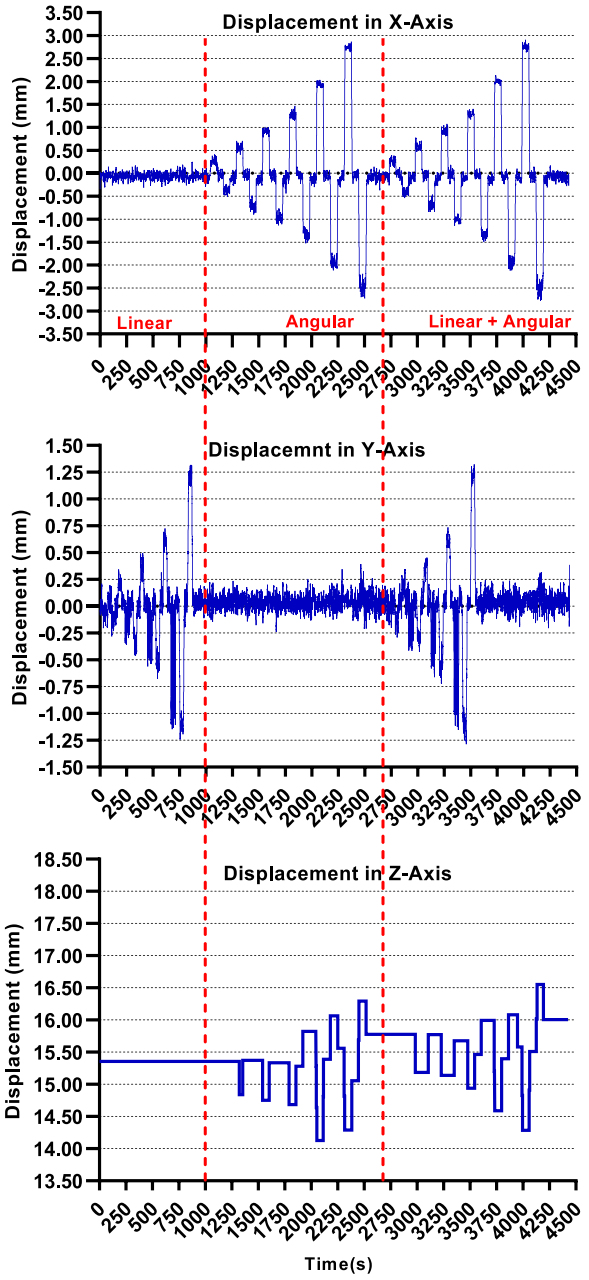


**FIGURE 17.** Quasi-static linear and angular movement.

date that can achieve 0.3 mm accuracy without the use of radiographs (RSA technique). Vibrometery has an accuracy of 20 % more than x-rays and the accuracy of standard radio graphs is 2 mm detection. The proposed detection technique has a much higher accuracy of detection (0.3 mm) without any radio graphic exposure.

Our current understanding of the mechanisms of loosening and its causes are still not entirely known due to the lack of continuous monitoring. The implications of developing this system for clinical use is that it could further our understanding of the dynamics of implant loosening behaviour in-situ, implant joint biomechanics and how implants are designed and managed long-term. However, the system has some limitations that need to be overcome.

One of the limitations in our system is the signal transmission and powering is currently wired. To address this was beyond the scope of this project as this was a proof-of-concept study aiming to investigate the feasibility of the system. This will be addressed in future work developing a compatible wireless signal transmission and powering system.

A second limitation is the tilt effect. There is no compensation for any non-parallel alignment between the sensor and the magnet. Currently the system carries out a calibration step to check the magnet and sensor are aligned and parallel before proceeding. Future work will be to develop the system to compensate for any starting mal alignment of the sensor and magnet by utilizing two or more sensors.

A third limitation is possible environmental effects. The system performance may be affected if it encounters an external magnetic field. The magnetic field strength decreases with the increase of distance. However, as long as the external magnetic field variations are at an appropriate distance from the sensor, it will not cause any disturbances to the sensor measurement.

## V. CONCLUSION

In this work, we have presented a proof-of-concept for a magnetic field-based system to detect the migration of a prosthesis as low as 0.3 mm for post-operative follow-up, using the humeral component of the elbow prosthesis as a case study to demonstrate the system. To the best of our knowledge this is the first magnetic-based system for prosthesis loosening detection without the use of radiographs and the first of its kind designed for understanding the loosening behavior of the humeral component in the elbow prosthesis with an achievable accuracy of 0.3 mm. This capability could have a significant impact on how implant loosening is monitored over the life span of the implant. This system potentially could have implications on understanding the dynamics of implant loosening behaviour in-situ, joint biomechanics and implant designs and how implants are managed long-term.

## REFERENCES


[1] N. Gschwend, B. R. Simmen, and Z. Matejovsky, "Late complications in elbow arthroplasty," *J. Shoulder Elbow Surg.*, vol. 5, no. 2, pp. 86–96, Mar. 1996.

[2] I. Voloshin, D. W. Schippert, S. Kakar, E. K. Kaye, and B. F. Morrey, "Complications of total elbow replacement: A systematic review," *J. Shoulder Elbow Surg.*, vol. 20, no. 1, pp. 158–168, Jan. 2011.

[3] C. P. Little, A. J. Graham, and A. J. Carr, "Total elbow arthroplasty," *J. Bone Joint Surg.*, vol. 87-B, no. 4, p. 437, 2005.

[4] A. Prkić, C. J. A. van Bergen, B. The, and D. Eygendaal, "Total elbow arthroplasty is moving forward: Review on past, present and future," *World. J. Orthopedics*, vol. 7, no. 1, pp. 44–49, Jan. 2016.

[5] C. L. Welsink, K. T. A. Lambers, D. F. P. van Deurzen, D. Eygendaal, and M. P. J. van den Bekerom, "Total elbow arthroplasty: A systematic review," *J. Bone Joint Surg.*, vol. 5, no. 7, p. e4, Jul. 2017.

[6] B.-T.-S. Fevang, S. A. Lie, L. I. Havelin, A. Skredderstuen, and O. Furnes, "Results after 562 total elbow replacements: A report from the norwegian arthroplasty register," *J. Shoulder Elbow Surg.*, vol. 18, no. 3, pp. 449–456, May 2009.

[7] E. T. Skyttä, A. Eskelinen, P. Paavolainen, M. Ikävalko, and V. Remes, "Total elbow arthroplasty in rheumatoid arthritis," *Acta Orthopaedica*, vol. 80, no. 4, pp. 472–477, Jan. 2009.

[8] S. B. Sneftrup, S. L. Jensen, H. V. Johannsen, and J. O. Søjbjerg, "Revision of failed total elbow arthroplasty with use of a linked implant," *J. Bone Joint Surg.*, vol. 88-B, no. 1, pp. 78–83, Jan. 2006.

[9] A. Dalemans, L. De Smet, and I. Degreef, "Long-term outcome of elbow resurfacing," *J. Shoulder Elbow Surg.*, vol. 22, no. 11, pp. 1455–1460, Nov. 2013.

[10] H. C. Plaschke, T. M. Thillemann, S. Brorson, and B. S. Olsen, "Implant survival after total elbow arthroplasty: A retrospective study of 324 procedures performed from 1980 to 2008," *J. Shoulder Elbow Surg.*, vol. 23, no. 6, pp. 829–836, Jun. 2014.

[11] Ø. Gøthesen, B. Espehaug, L. Havelin, G. Petursson, S. Lygre, P. Ellison, G. Hallan, and O. Furnes, "Survival rates and causes of revision in cemented primary total knee replacement," *Bone Joint J.*, vol. 95-B, no. 5, pp. 636–642, May 2013.

[12] M. Corradi, M. Frattini, B. Panno, S. Tocco, and F. Pogliacomi, "Linked semi-constrained total elbow prosthesis in chronic arthritis: Results of 18 cases," *Musculoskeletal Surg.*, vol. 94, no. S1, pp. 11–23, May 2010.

[13] M. Paterson, P. Fulford, and R. Denham, "Loosening of the femoral component after total hip replacement. The thin black line and the sinking hip," *J. Bone Joint Surg.*, vol. 68-B, no. 3, pp. 392–397, May 1986.

[14] A. Arami, J.-R. Delaloye, H. Rouhani, B. M. Jolles, and K. Aminian, "Knee implant loosening detection: A vibration analysis investigation," *Ann. Biomed. Eng.*, vol. 46, no. 1, pp. 97–107, Jan. 2018.

[15] A. H. Newberg and S. M. Wetzner, "Digital subtraction arthrography," *Radiology*, vol. 154, no. 1, pp. 238–239, Jan. 1985.

[16] B. S. Talbot and E. P. Weinberg, "MR imaging with metal-suppression sequences for evaluation of total joint arthroplasty," *Radiographics*, vol. 36, no. 1, pp. 209–225, Jan. 2016.

[17] C. N. B. Harisankar, B. R. Mittal, A. Bhattacharya, M. Parmar, and B. Singh, "Aseptic loosening of elbow prostheses diagnosed on F-18 FDG PET/CT," *Clin. Nucl. Med.*, vol. 35, no. 11, pp. 886–887, Nov. 2010.

[18] B. T. Brinke, A. Beumer, K. L. M. Koenraadt, D. Eygendaal, G. A. Kraan, and N. M. C. Mathijssen, "The accuracy and precision of radiostereometric analysis in upper limb arthroplasty," *Acta Orthopaedica*, vol. 88, no. 3, pp. 320–325, May 2017.

[19] J. C. T. van der Lugt, E. R. Valstar, S. W. Witvoet-Braam, and R. G. H. H. Nelissen, "Migration of the humeral component of the souter-strathclyde elbow prosthesis," *J. Bone Joint Surg.*, vol. 92-B, no. 2, pp. 235–241, Feb. 2010.

[20] E. R. Valstar, E. H. Garling, and P. M. Rozing, "Micromotion of the souter-strathclyde total elbow prosthesis in patients with rheumatoid arthritis," *Acta Orthopaedica Scandinavica*, vol. 73, no. 3, pp. 264–272, Jan. 2002.

[21] A. D. Rosenstein, G. F. McCoy, C. J. Bulstrode, P. D. McLardy-Smith, J. L. Cunningham, and A. R. Turner-Smith, "The differentiation of loose and secure femoral implants in total hip replacement using a vibrational technique: An anatomical and pilot clinical study," *Proc. Inst. Mech. Eng., H, J. Eng. Med.*, vol. 203, no. 2, pp. 77–81, Jun. 1989.

[22] G. Bergmann, F. Graichen, and A. Rohlmann, "Hip joint loading during walking and running, measured in two patients," *J. Biomech.*, vol. 26, no. 8, pp. 969–990, Aug. 1993.

[23] A. Arami, M. Simoncini, O. Atasoy, S. Ali, W. Hasenkamp, A. Bertsch, E. Meurville, S. Tanner, P. Renaud, C. Dehollain, P. Farine, B. M. Jolles, K. Aminian, and P. Ryser, "Instrumented knee prosthesis for force and kinematics measurements," *IEEE Trans. Autom. Sci. Eng.*, vol. 10, no. 3, pp. 615–624, Jul. 2013.

[24] M. Ahmed Khan, M. Serpelloni, and E. Sardini, "Optimized power harvesting module for an autonomous sensor system implanted in a total knee prosthesis," in *Proc. IEEE Int. Instrum. Meas. Technol. Conf. (IMTC)*, Turin, Italy, May 2017, pp. 1–6.

[25] H.-S. Hsiao, L.-Q. Chen, C.-K. Sung, and J.-Y. Chang, "Characteristics of magnetic sensor with assembly errors in a rotary recording system," *Microsyst. Technol.*, vol. 26, no. 1, pp. 89–94, Jan. 2020.

[26] P. Ripka and M. Janosek, "Advances in magnetic field sensors," *IEEE Sensors J.*, vol. 10, no. 6, pp. 1108–1116, Jun. 2010.

[27] A. Arami, J. Miehlbradt, and K. Aminian, "Accurate internal–external rotation measurement in total knee prostheses: A magnetic solution," *J. Biomech.*, vol. 45, no. 11, pp. 2023–2027, Jul. 2012.

[28] S. M. Aziz, M. Grcic, and T. Vaithianathan, "A real-time tracking system for an endoscopic capsule using multiple magnetic sensors," in *Smart Sensors and Sensing Technology*. Berlin, Germany: Springer, 2008, pp. 201–218.

[29] C. Schott, R. Racz, F. Betschart, and R. S. Popovic, "Novel magnetic displacement sensors," Tech. Rep. Sensors-00355, 2002.

[30] J. Lenz and S. Edelstein, "Magnetic sensors and their applications," *IEEE Sensors J.*, vol. 6, no. 3, pp. 631–649, Jun. 2006.

[31] C. Schott, F. Burger, H. Blanchard, and L. Chiesi, "Modern integrated silicon Hall sensors," *Sensor Rev.*, vol. 18, no. 4, pp. 252–257, Dec. 1998.
[32] R. Arora, "I2C bus pullup resistor calculation," Texas Instrum., Dallas, TX, USA, Appl. Rep. SLVA-689, Feb. 2015.
[33] M. Arora, E. K. S. Chan, S. Gupta, and A. D. Diwan, "Polymethylmethacrylate bone cements and additives: A review of the literature," *World J. Orthopedics*, vol. 4, no. 2, pp. 67–74, Apr. 2013.
[34] S. H. Goldberg, R. M. Urban, J. J. Jacobs, G. J. King, S. W. O'Driscoll, and M. S. Cohen, "Modes of wear after semiconstrained total elbow arthroplasty," *J. Bone Joint Surg.-Amer.*, vol. 90, no. 3, pp. 609–619, Mar. 2008.
[35] J. M. Camacho and V. Sosa, "Alternative method to calculate the magnetic field of permanent magnets with azimuthal symmetry," *Revista mexicana de física E*, vol. 59, no. 1, pp. 8–17, Jun. 2013.
[36] C. Hu, M. Q.-H. Meng, and M. Mandal, "A linear algorithm for tracing magnet position and orientation by using three-axis magnetic sensors," *IEEE Trans. Magn.*, vol. 43, no. 12, pp. 4096–4101, Dec. 2007.
[37] S. J. Orfanidis, "Signal processing application," in *Introduction to Signal Processing*, vol. 5, 1st ed. Upper Saddle River, NJ, USA: Prentice-Hall, 1995, ch. 8, sec. 3, pp. 427–452.
[38] L. U. Bigliani and E. V. Flatow, "Shoulder arthoplasty," in *Humeral Component Technique*, 1st ed. New York, NY, USA: Springer-Verlag, 2005, ch. 2, pp. 33–34.

**MUHAMMAD MOID KHALID KHAN** received the B.Sc. degree in electronic engineering from the University of Engineering and Technology, Peshawar, Pakistan, in 2012, and the M.Sc. degree in electrical engineering with power electronics from the University of Bradford, U.K., in 2015. He is currently pursuing the Ph.D. degree with the School of Engineering and Applied Science, Aston University, Birmingham, U.K. His research interests include embedded system applications, with an emphasis on magnetic sensor, chemical sensors, and wireless sensors.

**SUBODH C. DESHMUKH** has been a Consultant Orthopaedic and a Upper Limb Surgeon with City Hospital Birmingham, since September 1997, and a Consultant in Hand and Upper Surgery with The Royal Orthopaedic Hospital, Birmingham, since June 2003. He is also holding a position as an Honorary Clinical Senior Lecturer, University of Birmingham, and an Honorary Professor with Aston University, Birmingham. His education and training includes F.R.C.S. (Eng. and Glasgow), F.R.C.S. (orth), M.Ch. (orth), M.S. (orth), and D. Orth, M.B.B.S. He holds several academic positions, including being a member of the board of examiners for MRCS, RCPS Glasgow, (from 2002 to 2007), FRCS (orth), from 2008 to 2018, and a Diploma in Hand Surgery with the University of Manchester, since 2019.

**KANTHAN THEIVENDRAN** received the B.Sc. degree in orthopaedic science from University College London, in 2001, and the MBBS degree from Imperial College London, in 2003. He has undertaken prestigious higher surgical fellowship training in upper limb surgery from Derby and Wrightington. He currently practices as a Consultant Orthopaedic and Upper Limb Surgeon, specializing in shoulder and elbow and upper limb surgery, Birmingham, U.K. He is also an Honorary Professor with Aston University, Birmingham.

**LAURA J. LESLIE** received the B.Eng. degree in materials science and technology, the M.Sc. degree in medical engineering and biomechanics, and the Ph.D. degree in biomedical engineering. She is currently a Senior Lecturer and the Head of the Group in Mechanical Engineering and Design with Aston University, Birmingham, U.K. Her research interests include development and mechanical testing of medical devices and biomaterials, and replacement of animals in biomedical research.

**SARAH JUNAID** is currently a Senior Lecturer in mechanical engineering and design with Aston University and the Head of the Biomedical Engineering Research Unit. Her education and research training includes working in multidisciplinary teams with Imperial College London, University of Birmingham, and the University of Leeds. Her research interest includes orthopaedics, particularly in the longevity of joint replacements and improving fracture fixation treatment, with a background in finite element modeling, image processing, and mechanical tissue testing.